

RESEARCH ARTICLE



Synthesis and characterization of CZTS and $\text{Cu}_{2-x}\text{Ag}_x\text{ZnSnS}_4$ thin films for the application of solar cells

Kiran Kumari Pal¹, Pritam Sardar¹, Kamal Bhujel², Satyam Shankhdhar¹, Rajalingam Thangavel^{1*}

¹Department of Physics, IIT(ISM) Dhanbad, India. 826004

²Department of Physics, Mizoram University, Aizawl, India. 796009

We report on colloidal $\text{Cu}_2\text{ZnSnS}_4$ (CZTS) and $\text{Cu}_{2-x}\text{Ag}_x\text{ZnSnS}_4$ ($X=0.25$) nanoparticles synthesis by sol-gel spin coating process and hot injection method. The colloidal nanoparticles were deposited on ITO substrates by using spin-coating techniques. The deposited thin films were characterized by X-ray diffraction (XRD), UV-visible spectrometer, FE-SEM, Raman spectroscopy and Keithley 2450 Source meter. XRD reveals that the crystal structure of CZTS is confirmed tetragonal structure with peak (112) and observed the changes to wurtzite peak (002) due to the presence of Ag. UV visible spectra show that the optical band gap of CZTS nanoparticles decreases from 2 eV to around 1.75 eV, and there is a significant improvement in absorption coefficient when the sample is prepared under a nitrogen atmosphere. FESEM captured the microstructure image of CZTS and $\text{Cu}_{2-x}\text{Ag}_x\text{ZnSnS}_4$. Photoluminescence (PL) reveals the emission peaks and Raman spectra investigate the secondary phases present. XPS confirms the presence of each element and their oxidation state. Further, electrical properties are studied using the four-probe method at room temperature. CZTS offers optical and electrical properties, which allow it to be suitable for thin-film solar cell absorber layers, and Ag doping enhances its properties.

Received 27 Feb 2024

Accepted 31 Mar 2024

*For correspondence:
rthangavel@iitism.ac.in

Contact us:
mizoacadsci@gmail.com

Keywords : CZTS, colloidal nanoparticles, optical properties, spin coating, microstructure

Introduction

The world's requirement for energy is very large, and it can be met by non-renewable resources like fossil fuels, but their burning has a hazardous impact on the environment, and they are limited. Sun is an intense source of energy, and photovoltaics (PV) can bring in notable electricity from it.¹ One of the ways to utilize solar energy is thin film-based solar cells, which deploy various semiconductors as an absorber layer.² Copper Zinc Tin Sulphide (CZTS) is the emerging candidate for the same. $\text{Cu}_2\text{ZnSnS}_4$ (CZTS) is a quaternary semiconductor I-II-IV-VI₄ that exhibits p-type conductivity. It can be formed by replacing Selenium with Sulphur, the rare metal Indium, with Zinc and Tin in Copper Indium Sulphide (CIS). Each element of CZTS is abundant on Earth. It has an optical bandgap of nearly ~ 1.5 eV and a high absorption coefficient of $>10^4$ cm^{-1} , which matches well for the application of solar cells as an absorber

layer.³ Most of the elements are non-toxic, increasing their application worldwide.⁴

Presently, the PV market is ruled by Silicon Solar cells. Si possesses an indirect bandgap, and theoretically, its efficiency is idealized as 26.7%. They have a low absorption coefficient, high resistance to impurity, and require a thick layer, which results in high costs. On the other hand, CZTS is both cost-effective and environment-friendly.⁵ CZTS is also a thermoelectric substance with a high Seebeck coefficient but a very low thermal and electrical conductivity.⁶ Research showed that we can replace intrinsic ions of CZTS with extrinsic ions (cations) to improve their properties.⁷ Researchers are focusing on CZTS devices, and reports show that CZTS-based solar cell devices reached an efficiency of 12.6%.⁴ There are numerous ways to synthesize CZTS,⁸

including spray pyrolysis,⁹ hydrazine solution of CZTS,¹⁰ hot injection method,¹¹ thermal co-evaporation,¹² sputtering,¹³ electrodeposition,¹⁴ a sol-gel technique¹⁵. In recent studies, due to its non-toxic nature, CZTS has been identified as a useful material for photovoltaic applications.^{16,17} In the past few years, various research and work have been done to upgrade the conversion efficiency of the absorber layer in 2D solar cells through various chemical changes. Chemical changes in CZTS (i.e., limited replacement of base material) may improve its efficiency as an absorber layer. In this work, we synthesized CZTS and $\text{Cu}_{2-x}\text{Ag}_x\text{ZnSnS}_4$ nanoparticles by sol-gel and hot-injection methods. Further, to study the properties of these nanoparticles, we prepare thin films.

Materials and methods

Materials

Copper chloride dihydrate ($\text{CuCl}_2 \cdot 2\text{H}_2\text{O}$, MW = 170.446 g/mol), zinc chloride dry (ZnCl_2 , MW = 136.286 g/mol), tin chloride dihydrate ($\text{SnCl}_2 \cdot 2\text{H}_2\text{O}$, MW = 225.616 g/mol), thiourea ($\text{NH}_2 \cdot \text{CS} \cdot \text{NH}_2$, MW = 76.12 g/mol), Acetone and Ethanol were purchased from MERCK, Germany. 2-methoxyethanol monoethanolamine (MEA), Hexene (C_6H_{12}) and Toluene (C_7H_8) were purchased from Alfa Aesar, United States. Silver Nitrate (AgNO_3 , MW = 169.87 g/mol) was purchased from RANKEM, India. ITO glass substrates are used for thin film coating.

Sample preparation

For the synthesizing of colloidal CZTS and $\text{Cu}_{2-x}\text{Ag}_x\text{ZnSnS}_4$, we employed sol-gel and hot-injection techniques. The molar concentration of specific elements in the two solutions was quite different. In the sol-gel process, 1 mol of Copper chloride dihydrate ($\text{CuCl}_2 \cdot 2\text{H}_2\text{O}$), 0.5 mol of Zinc chloride dry (ZnCl_2), 0.5 mol of Tin chloride dihydrate ($\text{SnCl}_2 \cdot 2\text{H}_2\text{O}$), 6 mol of thiourea ($\text{NH}_2 \cdot \text{CS} \cdot \text{NH}_2$; MERCK) were dissolved in 20 ml of 2-methoxy ethanol one by one along with stirring at room temperature (600rpm) and the temperature was build up to 50°C for 1 hour to obtain a homogeneous solution of CZTS. Further, for $\text{Cu}_{2-x}\text{Ag}_x\text{ZnSnS}_4$ preparation, the process is repeated, and 0.5 mol of Silver nitrate (AgNO_3) is added. In the hot-injection method, 30ml of oleylamine was taken in the three-neck flask, fitted to the schlenk line and metal heating mental. Then, all the precursors were added one by one except thiourea. All the opening of the three-neck flask was closed. 5 ml of thiourea was injected into the flask with the help of a needle and syringe. The final solution was degassed for 10 minutes, and the temperature was increased to 160°C. Finally, the solution was purged with nitrogen gas three times, and the blue solution turned black. The temperature was increased to 230°C for 30 minutes in a nitrogen atmosphere. This method obtained a dark black viscous solution of CZTS. Ink solutions were then

centrifuged in hexene and acetone to obtain CZTS nanoparticles, which were then dispersed in toluene and stored at room temperature. For the preparation of thin films, we proceed towards a non-vacuum sol-gel deposition technique using a spin coater because vacuum-based approaches require unreasonable energy, low material implementation, and high prices.¹⁸

Thin film preparation

ITO substrate of dimension 1 cm X 1 cm was used for the purpose of thin films. First, substrates were cleaned ultrasonically using piranha solution for 20 minutes and then by De-ionised (DI) water, acetone, DI water, ethanol, and DI water in a row each for 20 minutes and then substrate were allowed to dry in the oven for 30 minutes at 60° C. Then, substrates are coated with thin films of prepared solutions using a spin coater at 3000 rpm with a control time of 30 seconds. The substrate was then dried on the hot plate for 10 minutes at 150° C and then in the oven at 250° C. Coating was done 10 times on each layer.

Characterizations

The crystal structure of both CZTS and $\text{Cu}_{2-x}\text{Ag}_x\text{ZnSnS}_4$ was analyzed by a High-Resolution X-Ray Diffraction facility with a Rigaku Oxford diffraction system with state of art CCD Eos S2 detector (XRD).¹⁹ Field Emission Scanning Electron Microscopy (FESEM, Carl Zeiss, model supra 55) captured the microstructures of the samples. The optical properties of the samples were analyzed by UV-VIS-NIR spectrophotometer (Agilent Cary 5000), emission properties were revealed by Photoluminescence (PL) spectra which employed 325 nm laser and for further investigation of secondary phases Raman spectra were captured which employs 532 nm laser in LabRAM HR-UV-Open Micro-Raman Spectroscopy, HORIBA scientific, France and electrical properties were investigated with Keithley 2450 Model. For electrical characterization purposes, the four-probe method at room temperature was used. The four contact terminals of the Keithley 2450 device were put on an area of 1 cm x 1 cm of thin films.²⁰ For chemical composition and oxidation state, X-ray photoelectron Spectroscopy (XPS) with 5000 verse probe III, PHI is employed. The thickness of thin films was calculated using a Dektak XT surface profilometer

Results and discussion

Structural

XRD

HR-XRD spectra of CZTS samples prepared by sol-gel and hot injection techniques were recorded by the Rigaku Oxford Diffraction system in scanning from 20°-70° with a step size of 0.02°.

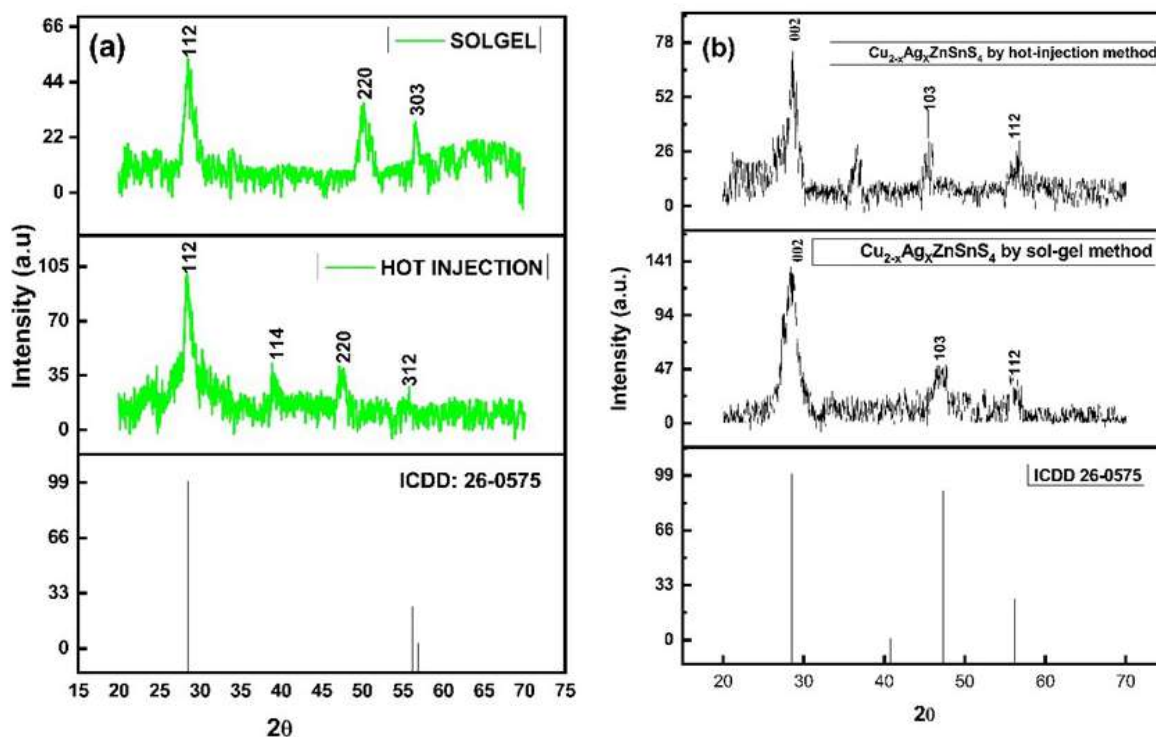


Figure 1. XRD spectra of CZTS (a) and $\text{Cu}_{2-x}\text{Ag}_x\text{ZnSnS}_4$ (b) prepared by sol-gel and hot injection method and its comparison with ICDD data

The prominent peaks of the CZTS sample prepared by sol-gel are 28.56° , 47.73° , and 56.02° ²¹ which are assigned to (112), (220) and (303) hkl planes and peaks of the CZTS sample prepared by hot injection are 28.53° , 40.74° , 47.32° and 56.02° ²² which are assigned to (112), (114), (220), and (312), peaks of $\text{Cu}_{2-x}\text{Ag}_x\text{ZnSnS}_4$ prepared by sol-gel method are 28.56° , 47.73° , and 56.02° which are assigned to (002), (103) and (112) while peaks of $\text{Cu}_{2-x}\text{Ag}_x\text{ZnSnS}_4$ prepared by hot-injection method are 28.56° , 41.1° , 47.73° , and 56.02° which are assigned to (002), (103) and (112) with an unknown peak at (41.1°). An unknown peak may be due to an amorphous nature.²³ All these peaks agree with the International Centre of Diffraction Data, which corresponds to a tetragonal structure in CZTS and a wurtzite structure in $\text{Cu}_{2-x}\text{Ag}_x\text{ZnSnS}_4$. Diffraction peaks of CZTS and $\text{Cu}_{2-x}\text{Ag}_x\text{ZnSnS}_4$ prepared by sol-gel and hot injection differ in intensities and shapes, as shown in Fig. 1. Hot injection shows sharper and more intense peaks compared to the sol-gel sample, which indicated a higher degree of crystallinity and improved phase purity.²⁴ Crystallite size was examined using Debye-Scherrer's formula with the help of full-width half maxima (FWHM) values of the dominant peak in both samples.

$$D = \frac{K\lambda}{\beta \cos\theta} \quad (1)$$

Where D is crystallite size, K is Scherrer's constant, i.e. 0.9, λ is the wavelength of X-rays, i.e. 1.54\AA , θ is Bragg angle, and β is full-width half maxima (FWHM). Through Lorentzian fit, FWHM values of

Table 1. Variation of crystallite size with FWHM

Film sample	FWHM (β)	D (nm)
CZTS by sol-gel	0.024	57
CZTS by Hot injection	0.014	92
$\text{Cu}_{2-x}\text{Ag}_x\text{ZnSnS}_4$ by sol-gel method	0.117	16
$\text{Cu}_{2-x}\text{Ag}_x\text{ZnSnS}_4$ by hot-injection method	0.408	32

CZTS prepared by sol-gel and hot injection are shown above in Table 1.

The crystallite size of CZTS by sol-gel came out to be 57 nm, whereas the hot injection sample has a larger crystallite size of around 92 nm, while $\text{Cu}_{2-x}\text{Ag}_x\text{ZnSnS}_4$ shows a large reduction in crystallite size. The difference in crystallite size can be due to controlled condensation and hydrolysis in sol-gel, while crystallite size in the hot injection technique is larger, which can be due to rapid nucleation and growth kinetic. Crystallographic parameters (a, b and c) were calculated by matching the 2θ values of hkl with ICDD data using the following equation:

$$\frac{1}{d^2} = \frac{h^2 + k^2}{a^2} + \frac{l^2}{c^2} \quad (2)$$

where (hkl) are miller indices of XRD peaks, where d is lattice plane space. Crystallographic parameters a and b were 5.42\AA and c was 10.93\AA which accord well with the ICDD data of CZTS (a = b = 5.43\AA , c = 10.843\AA), and this confirms the

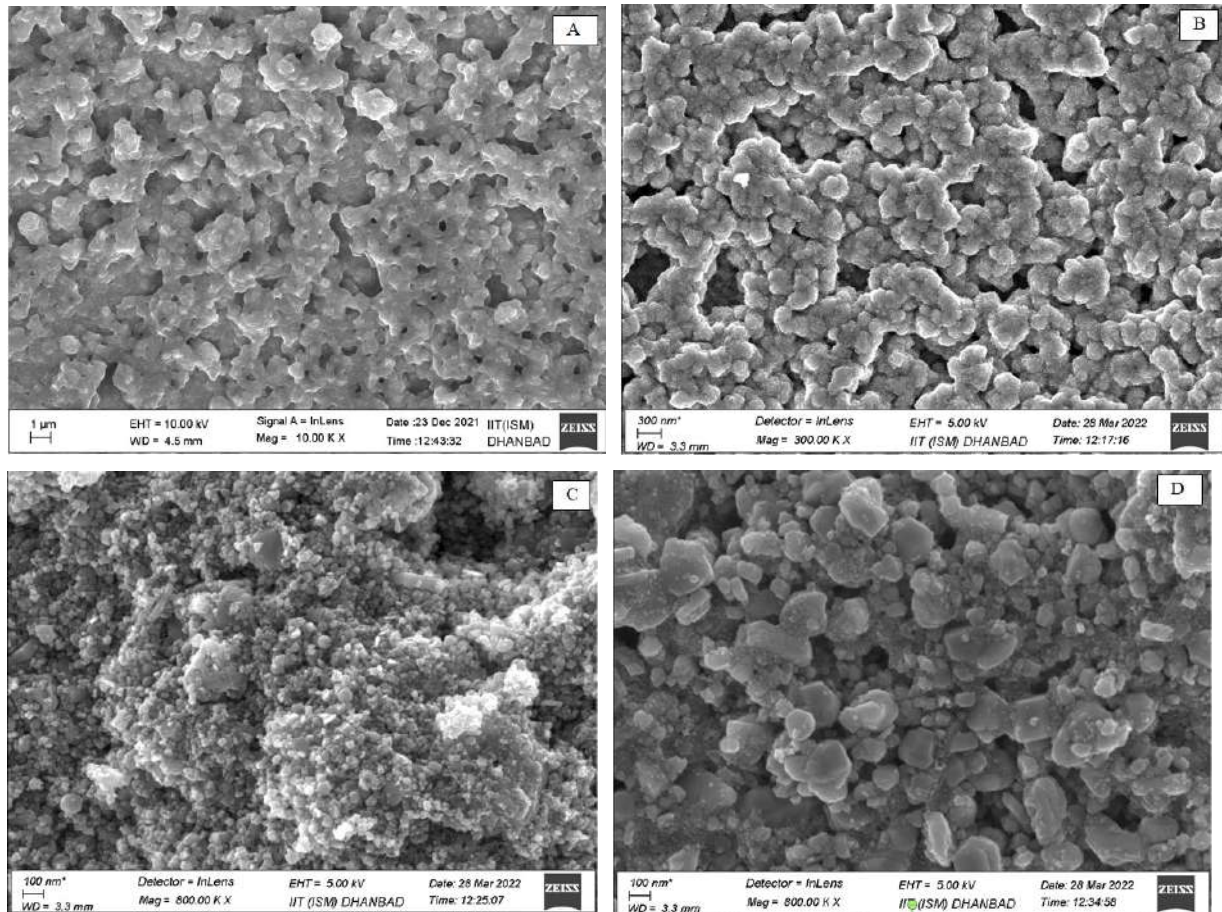


Figure 2. FESEM image of CZTS by (A) Sol-gel method (C) Hot-injection method and $\text{Cu}_{1.75}\text{Ag}_{0.25}\text{ZnSnS}_4$ (B) Sol-gel method (D) Hot-injection method

tetragonal structure of CZTS sample prepared by both techniques.

Morphology

FESEM

To study the surface morphology of prepared CZTS and $\text{Cu}_{2-x}\text{Ag}_x\text{ZnSnS}_4$ thin films, micrographs were captured using FE-SEM at 1 μm , 100 nm and 300 nm resolution. We choose specific magnification because of the existence of quite compact nanoparticles, which may be due to the sulphurisation of the sample during solution preparation and annealing. Fig 2 reveals a top view of FESEM images.²⁵ Grain boundaries are clearly visible in samples with Ag doping and the one prepared by the hot injection method compared to pure CZTS.²⁶

Vast difference in film thickness

The shades of TFs assembled by spin-coating are black.²⁷ The film thickness of CZTS for samples by sol-gel and hot-injection are 2106.743 and 267.74 nm, respectively, while for $\text{Cu}_{2-x}\text{Ag}_x\text{ZnSnS}_4$ the TFs thickness is 815.81 nm and 98.663 nm for sol-gel and hot-injection respectively. This large variation may be due to better sulphurisation in

samples by the hot-injection method, as it is prepared under a nitrogen atmosphere. Moreover, analysis reveals that nucleation may be more complex in the latter case.²⁸

Optical properties

Absorption coefficient and band gap calculation

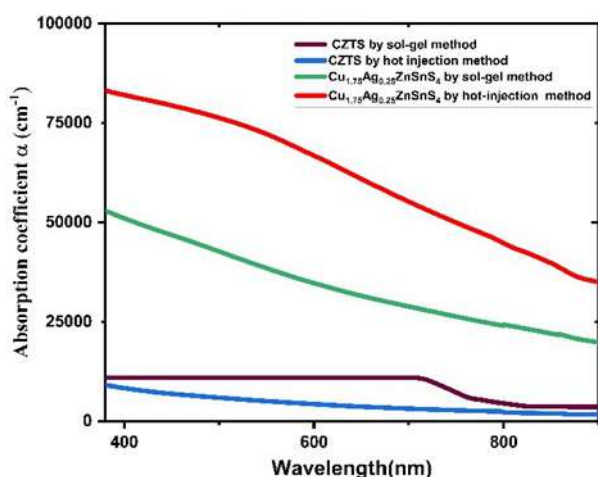
Fig. 3 reveals Absorbance of CZTS and $\text{Cu}_{2-x}\text{Ag}_x\text{ZnSnS}_4$ prepared by the hot-injection method. $\text{Cu}_{2-x}\text{Ag}_x\text{ZnSnS}_4$ depicts a higher absorption coefficient α as compared to CZTS. The large value of α for Ag doping shows that thin films take in most radiations falling on them.²⁹ A value of α around 10^4 holds up the direct band gap essence of CZTS.³⁰ Further, using α , the band gap is calculated. The tauc formula for the calculation of the optical band gap is given by

$$\alpha hv = A(hv - E_g)^n \quad (3)$$

Where E_g = optical band gap of sample, A = constant hv is inclined energy on film, and $n = 1/2$ as CZTS is a direct band gap semiconductor reported by Ghosh *et. al.*³¹. Fig. 4 represents $(\alpha hv)^2$ vs. energy graph of all the samples. Determination of band gap was done by extending the linear variation of the graph. Analysis revealed that the

Table 2: Variation of bandgap, film thickness, resistance, and resistivity by sol-gel and hot-injection method

Film samples	Bandgap (eV)	Film thickness (nm)	Resistance (Ω)	Resistivity (Ωm)
CZTS by sol-gel	2	2106.74	4.30×10^7	9.058×10^{-3}
CZTS by Hot injection	1.95	267.74	696.92	0.019
$\text{Cu}_{2-x}\text{Ag}_x\text{ZnSnS}_4$ by sol-gel method	1.85	815.81	1.81×10^8	14.770×10^{-3}
$\text{Cu}_{2-x}\text{Ag}_x\text{ZnSnS}_4$ by hot-injection method	1.75	98.66	4646.15	0.044

**Figure 3.** The absorption coefficient of CZTS and $\text{Cu}_{1.75}\text{Ag}_{0.25}\text{ZnSnS}_4$

band gap varies from 2 eV to 1.75 eV. The band gap decrease in doped samples may be due to crystal formation, as seen by FESEM images. The observed bandgap is higher than the theoretical value for CZTS ~ 1.45 eV; it may be due to various phases of these films, which XRD cannot discover because CZTS is not crystallized to a great extent as solutions are prepared at 230°C , rise in temperature can lead to a reduction in band gap.³² The variation in the band gap is summarized in Table 2.

Photoluminescence

Fig.5. represents the Photoluminescence (PL) spectra of CZTS and the effect of Ag doping. The intense peaks are observed at 523 and 497 nm for the samples CZTS and $\text{Cu}_{2-x}\text{Ag}_x\text{ZnSnS}_4$ by sol-gel method, while for samples CZTS and $\text{Cu}_{2-x}\text{Ag}_x\text{ZnSnS}_4$ by hot injection method, intense peaks are observed at 498 and 500 nm respectively. Other minor peaks are also observed in the visible region, indicating band-to-band emission of CZTS.³³ From Fig.5, we observed that the intensity of PL emission increases as the particle size decreases, indicating that intensity increases with doping.

Raman spectra

Raman spectra were analyzed in search of secondary phases present in the samples.³⁴ Raman spectra of CZTS and $\text{Cu}_{2-x}\text{Ag}_x\text{ZnSnS}_4$ are shown in Fig.6. Himmrich and Haeuseler³⁵ in 1991 show that in chalcopyrites, vibrations are found near 300 cm^{-1} and vary a little due to the vibration of the Sulphur atom only. From Fig.6, it is clear that the strongest peaks are between $328\text{--}333\text{ cm}^{-1}$, which confirms A1 symmetry.³⁶ Weak peaks at 423 cm^{-1} , 506 cm^{-1} , and 428 cm^{-1} are present in the samples prepared by hot injection method and one at 416 cm^{-1} for CZTS by sol-gel. It may be due to the Cu_{2-x}S phase present in the sample, as most of the Cu_{2-x}S compounds have their intense peak around 475 cm^{-1} .³⁷

Electrical properties

Fig.7 shows IV characteristics of grown CZTS and $\text{Cu}_{2-x}\text{Ag}_x\text{ZnSnS}_4$ TFs by two methods. the calculations can be done for the sheet resistance and resistivity using the equation –

$$R = \beta \frac{V}{I} \quad (4)$$

Resistivity is given by-

$$P = Rt \quad (5)$$

here, R represents sheet resistance, ρ represents resistivity, β is a constant having a value of 4.53, V is the applied voltage, and I represents current, where t is the film thickness.³⁸ As per measurement, the resistance and resistivity of the thin film prepared by both methods are represented in Table 2.³⁹

Resistivity decreased when we switched to the hot injection method both in the case of doped and Ag-doped CZTS, Ag substituted Cu atom to decrease CuZn antisite due to which the emergence energy of AgZn defect is much more than CuZn, so doping reduces defects in the crystal. If instead of one we substitute two atoms, then we can improve the conductivity of CZTS further.⁷

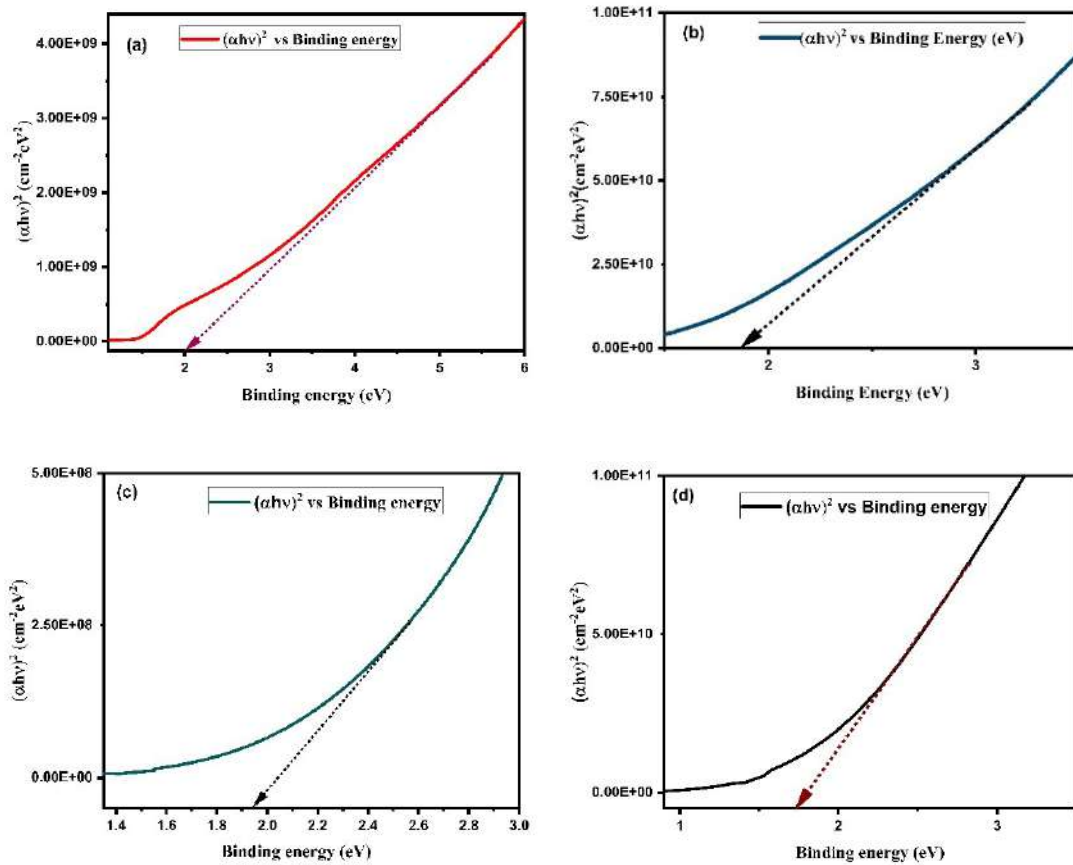


Figure 4. Tauc plot of CZTS (a) by sol-gel method (c) by hot-injection method and $\text{Cu}_{1.75}\text{Ag}_{0.25}\text{ZnSnS}_4$ (b) Sol-gel method (d) Hot-injection method

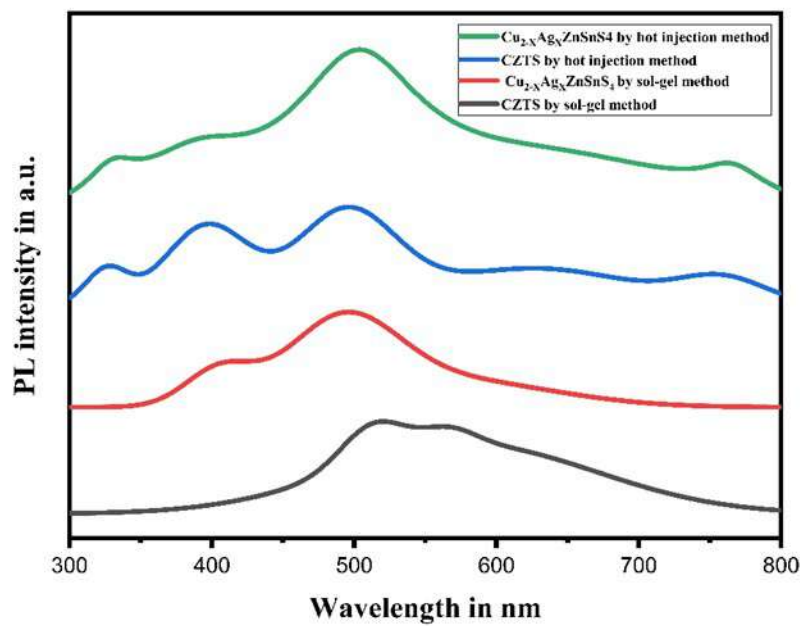


Figure 5. PL graph of CZTS and $\text{Cu}_{2-x}\text{Ag}_x\text{ZnSnS}_4$

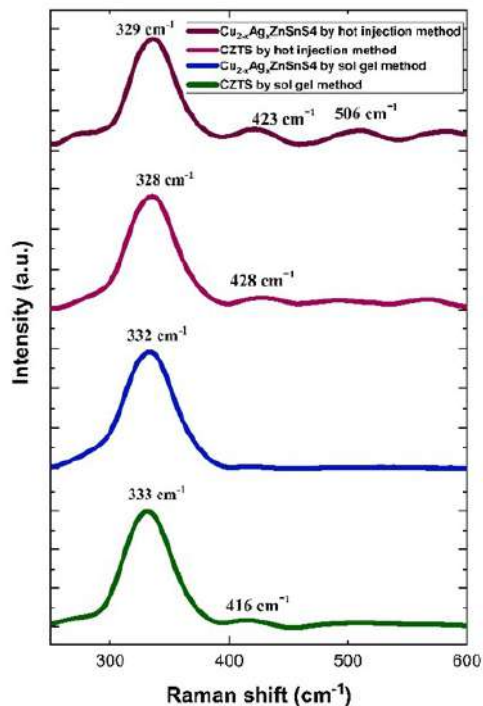


Figure 6. Raman spectra of CZTS and $\text{Cu}_{2-x}\text{Ag}_x\text{ZnSnS}_4$

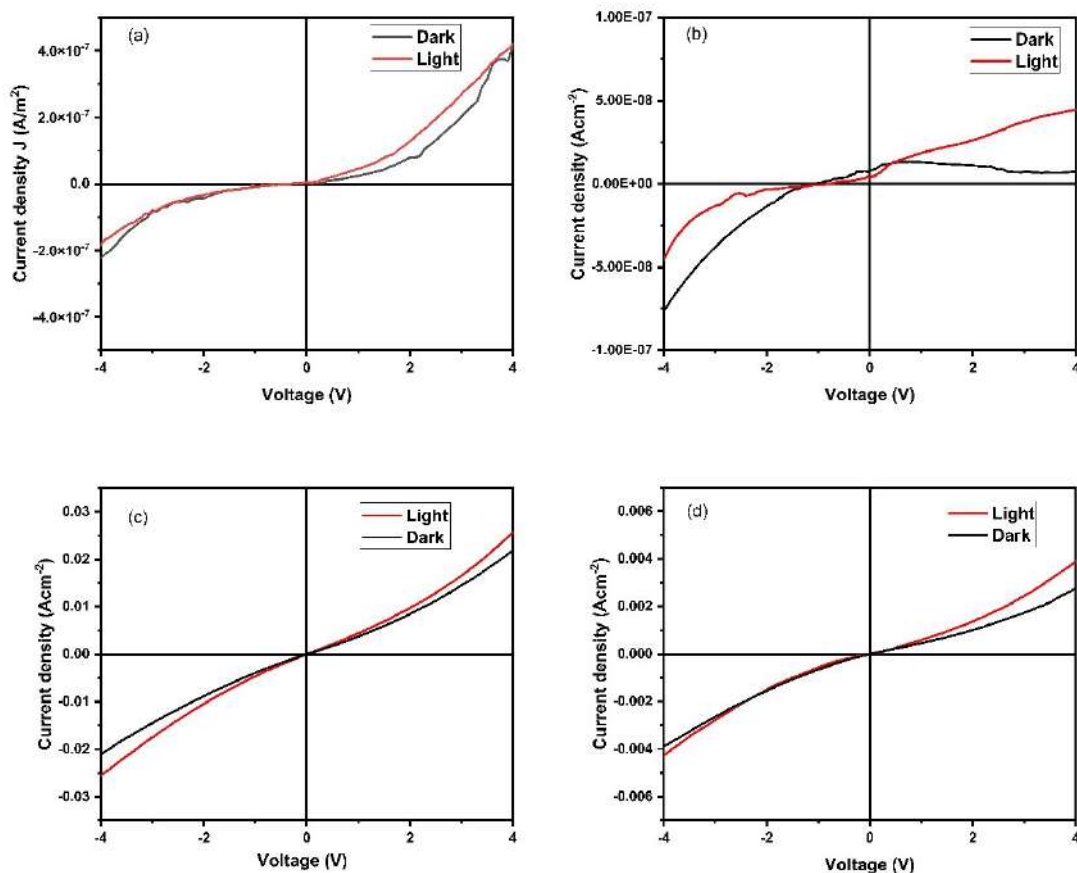


Figure 7. I-V characteristics of CZTS by (a) sol-gel method, (c) hot-injection method and $\text{Cu}_{1.75}\text{Ag}_{0.25}\text{ZnSnS}_4$ (b) Sol-gel method, (d) Hot-injection method

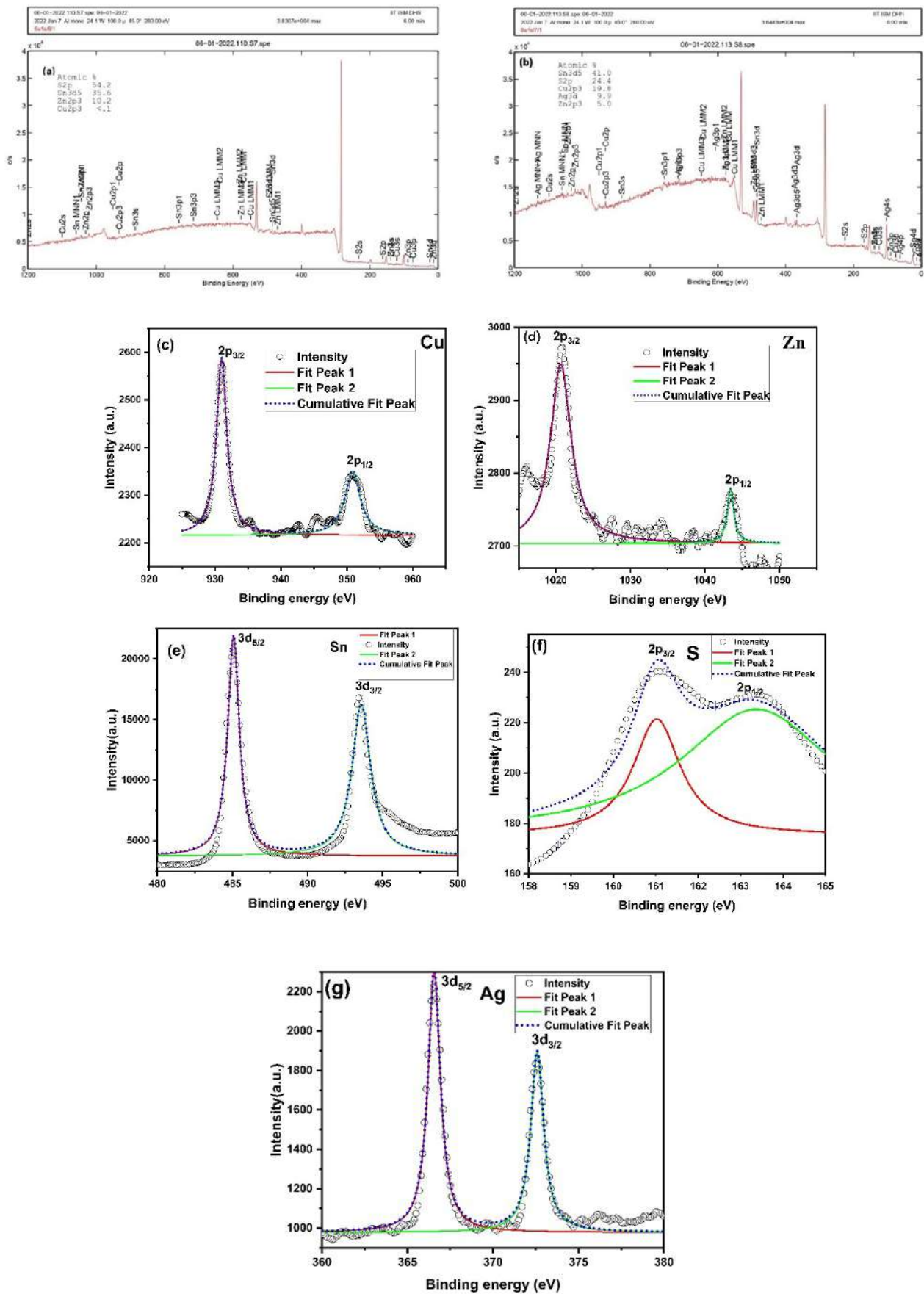


Figure 8. XPS spectra of CZTS and Cu_{2-x}Ag_xZnSnS₄

XPS

Fig. 8. (a) and (b) show broad scan of CZTS and $\text{Cu}_{2-x}\text{Ag}_x\text{ZnSnS}_4$ respectively and peaks of Cu2p, Zn2p, Sn3d, S2p, Ag3d while Fig. 8. (c),(d), (e),(f) and (g) show core spectra of each element. Fig. 8 (c) indicates two peaks at 931.1 eV (2p3/2) and 950.29 eV (2p1/2) with a separation of 19.19 eV which confirms its +1 valence state.⁴⁰ Fig. 8(d) represents Zn core level spectra with peaks at 1020.5 eV (2p3/2) and 1043.3 eV (2p1/2) with a separation of 22.8 eV which confirms Zn in +2 valence state. Sn spectra (Fig. 8 (e)) with a separation of 8.415 eV confirm its presence as Sn (IV). Peaks of S do not split properly, curve fitting shows the separation of 2.3 eV which confirms it in sulphide phase.⁴¹ Ag peaks (3d5/2 and 3d3/2) with a separation of 6.15 eV confirms +1 state of Ag.⁴²

Conclusion

We deposited CZTS and $\text{Cu}_{2-x}\text{Ag}_x\text{ZnSnS}_4$ thin films on an ITO substrate. The XRD analysis confirms that crystal structure changes from tetragonal to wurtzite as we proceed from CZTS to $\text{Cu}_{2-x}\text{Ag}_x\text{ZnSnS}_4$. The crystallite size is less in $\text{Cu}_{2-x}\text{Ag}_x\text{ZnSnS}_4$ by both methods. The reduction in crystallite size may be due to hydrolysis in the sol-gel method. FESEM images revealed that grain boundaries are clearly visible in Ag-doped CZTS. From UV-visible analysis, we concluded that $\alpha \geq 104 \text{ cm}^{-1}$ in the case of Ag doping and around 10^4 cm^{-1} in undoped samples, which makes it an appropriate thin film for photovoltaics. Further, bandgap decreases from 2 eV to 1.75 eV due to Ag presence. We can conclude band-to-band emission and the presence of the Cu_{2-x}S phase from PL and Raman spectra. The electrical resistivity shows higher conductivity in samples prepared by the hot-injection method. XPS confirms the presence of Cu, Zn, Sn and Ag in +1, +2, +4 and +1 oxidation states, respectively and S in the sulphide phase. The construction of $(\text{Cu}_{2-x}\text{Ag}_x\text{ZnSnS}_4/\text{ZnO})$ type solar cell is required to study quantum efficiency and for later work. From structural, optical, and electrical properties, we summarize that the properties of CZTS can be improved by replacing intrinsic ions with extrinsic ions (cations) and using them as one of the potential layers for application in solar cells.

Acknowledgements

The authors of this paper are thankful to the Central Research Faculty, Department of Physics IIT (ISM) Dhanbad. Heartfelt thanks to Prof. R. Thangavel for providing all the research support.

References

1. Khalate, S.A., Kate, R.S., Deokate, R.J. (2018). A review on energy economics and the recent research and development in energy and the

$\text{Cu}_2\text{ZnSnS}_4$ (CZTS) solar cells: A focus towards efficiency. *Solar Energy*, **169**, 616–633. <https://doi.org/10.1016/j.solener.2018.05.036>

2. Ananthoju, B., Mohapatra, J., Bahadur, D., Medhekar, N.V., Aslam, M. (2019). Influence of the $\text{Cu}_2\text{ZnSnS}_4$ nanoparticles size on solar cell performance. *Solar Energy Materials and Solar Cells*, **189**, 125–132. <https://doi.org/10.1016/j.solmat.2018.09.028>
3. Swami, S.K., Kumar, A., Dutta, V. (2013). Deposition of kesterite $\text{Cu}_2\text{ZnSnS}_4$ (CZTS) thin films by spin coating technique for solar cell application. *Energy Procedia*, **33**, 198–202. <https://doi.org/10.1016/j.egypro.2013.05.058>
4. Mahajan, S., Stathatos, E., Huse, N., Birajdar, R., Kalarakis, A., Sharma, R. (2018). Low cost nanostructure kesterite CZTS thin films for solar cells application. *Materials Letters*, **210**, 92–96. <https://doi.org/10.1016/j.matlet.2017.09.001>
5. Nazligul, A.S., Wang, M., Choy, K.L. (2020). Recent development in earth-abundant kesterite materials and their applications. *Sustainability* **12** (12), 5138. <https://doi.org/10.3390/su12125138>
6. Sharma, S.D., Khasimsaheb, B., Chen, Y.Y., Neeleshwar, S. (2019). Enhanced thermoelectric performance of $\text{Cu}_2\text{ZnSnS}_4$ (CZTS) by incorporating Ag nanoparticles. *Ceramics International*, **45**(2), 2060–2068. <https://doi.org/10.1016/j.ceramint.2018.10.109>
7. Qiu, L., Xu, J., Tian, X. (2019). Fabrication of ag and mn co-doped $\text{Cu}_2\text{ZnSnS}_4$ thin film. *Nanomaterials*, **9**(11). <https://doi.org/10.3390/nano9111520>
8. Huang, T.J., Yin, X., Qi, G., Gong, H. (2014). CZTS -based materials and interfaces and their effects on the performance of thin film solar cells. *Physica Status Solidi - Rapid Research Letters*, **8**(9), 735–762. <https://doi.org/10.1002/pssr.201409219>
9. Aono, M., Yoshitake, K., Miyazaki, H. (2013). XPS depth profile study of CZTS thin films prepared by spray pyrolysis. *Physica Status Solidi (C) Current Topics in Solid State Physics*, **10**(7–8), 1058–1061. <https://doi.org/10.1002/pssc.201200796>
10. Song, Z., Phillips, A.B., Xie, Y., Khanal, R.R., Stone, J.M., Heben, M.J. (2014). The Effect of Substrate Wettability on Hydrazine-Processed CZTS Thin Films. *Materials Research Society Symposium Proceedings*, **1648**.

11. Bade, B.R., Rondiya, S.R., Jadhav, Y.A., Kamble, M.M., Barma, S.V., Jathar, S.B., Nasane, M.P., Jadkar, S.R., Funde, A.M., Dzade, N.Y. (2021). Investigations of the structural, optoelectronic and band alignment properties of $\text{Cu}_2\text{ZnSnS}_4$ prepared by hot-injection method towards low-cost photovoltaic applications. *Journal of Alloys and Compounds*, **854**. <https://doi.org/10.1016/j.jallcom.2020.157093>
12. Tombak, A., Ocak, Y.S., Genişel, M.F., Kilicoglu, T. (2014). Electrical and optical properties of $\text{Cu}_2\text{ZnSnS}_4$ grown by a thermal co-evaporation method and its diode application. *Materials Science in Semiconductor Processing*, **28**, 98–102. <https://doi.org/10.1016/j.mssp.2014.07.006>
13. Gour, K.S., Yadav, A.K., Singh, O.P., Singh, V.N. (2018). Na incorporated improved properties of $\text{Cu}_2\text{ZnSnS}_4$ (CZTS) thin film by DC sputtering. *Vacuum*, **154**, 148–153. <https://doi.org/10.1016/j.vacuum.2018.05.007>
14. Boudaira, R., Meglali, O., Bouraiou, A., Attaf, N., Sedrati, C., Aida, M.S. (2020). Optimization of sulphurization temperature for the production of single-phase CZTS kesterite layers synthesized by electrodeposition. *Surface Engineering*, **36(9)**, 1000–1011. <https://doi.org/10.1080/02670844.2020.1758013>
15. Benachour, M.C., Bensaha, R., Moreno, R. (2019). Annealing duration influence on dip-coated CZTS thin films properties obtained by sol-gel method. *Optik*, **187**, 1–8. <https://doi.org/10.1016/j.ijleo.2019.05.015>
16. Méndez-López, A., Morales-Acevedo, A., Acosta-Silva, Y.J., Ortega-López, M. (2016). Synthesis and Characterization of Colloidal CZTS Nanocrystals by a Hot-Injection Method. *Journal of Nanomaterials*, **2016**. <https://doi.org/10.1155/2016/7486094>
17. Krishnan, A., Ali, R.K., Vishnu, G., Kannan, P. (2019). Towards phase pure CZTS thin films by SILAR method with augmented Zn adsorption for photovoltaic applications. *Materials for Renewable and Sustainable Energy*, **8(3)**. <https://doi.org/10.1007/s40243-019-0152-1>
18. Suryawanshi, M.P., Agawane, G.L., Bhosale, S.M., Shin, S.W., Patil, P.S., Kim, J.H., Moholkar, A.V. (2013). CZTS based thin film solar cells: A status review. *Materials Technology*, **28 (1-2)**, 98–109. <https://doi.org/10.1179/1753555712Y.0000000038>
19. <https://www.iitism.ac.in/deans/research/crf/base.php?instrument=SC-XRD>
20. Mwathe, P., Musembi, R., Munji, M., Odari, V., Munguti, L., Ntilakigwa, A., Nguu, J., Muthoka, B. (2014a). Effect of surface passivation on electrical properties of Pd-F: SnO₂ thin films prepared by spray pyrolysis technique. *Coatings*, **4(4)**, 747–755. <https://doi.org/10.3390/coatings4040747>
21. Yu, X., Ren, A., Wang, F., Wang, C., Zhang, J., Wang, W., Wu, L., Li, W., Zeng, G., Feng, L. (2014). Synthesis and characterization of CZTS thin films by sol-gel method without sulfurization. *International Journal of Photoenergy*, **2014**. <https://doi.org/10.1155/2014/861249>
22. Wang, W., Winkler, M.T., Gunawan, O., Gokmen, T., Todorov, T.K., Zhu, Y., Mitzi, D.B. (2014). Device characteristics of CZTSSe thin-film solar cells with 12.6% efficiency. *Advanced Energy Materials*, **4(7)**. <https://doi.org/10.1002/aenm.201301465>
23. Shin, S.W., Pawar, S.M., Park, C.Y., Yun, J.H., Moon, J.H., Kim, J.H., Lee, J.Y. (2011). Studies on $\text{Cu}_2\text{ZnSnS}_4$ (CZTS) absorber layer using different stacking orders in precursor thin films. *Solar Energy Materials and Solar Cells*, **95(12)**, 3202–3206. <https://doi.org/10.1016/j.solmat.2011.07.005>
24. Xia, D., Zheng, Y., Lei, P., Zhao, X. (2013). Characterization of $\text{Cu}_2\text{ZnSnS}_4$ thin films prepared by solution-based deposition techniques. *Physics Procedia*, **48**, 228–234. <https://doi.org/10.1016/j.phpro.2013.07.036>
25. Sripan, C., Alagarasan, D., Varadharajaperumal, S., Ganesan, R., Naik, R. (2020). Influence of solvent on solution processed $\text{Cu}_2\text{ZnSnS}_4$ nanocrystals and annealing induced changes in the optical, structural properties of CZTS film. *Current Applied Physics*, **20(8)**, 925–930. <https://doi.org/10.1016/j.cap.2020.05.003>
26. Prabeesh, P., Saritha, P., Selvam, I.P., Potty, S.N. (2017). Fabrication of CZTS thin films by dip coating technique for solar cell applications. *Materials Research Bulletin*, **86**, 295–301. <https://doi.org/10.1016>
27. Chtouki, T., Soumahoro, L., Kulyk, B., Bougharraf, H., Erguig, H., Ammous, K., Sahraoui, B. (2017). Comparative Study on the Structural, Morphological, Linear and Nonlinear Optical Properties of CZTS Thin Films Prepared

- by Spin-Coating and Spray Pyrolysis. *Materials Today: Proceedings*, **4(4)**, 5146–5153. <https://doi.org/10.1016/j.matpr.2017.05.020>
28. Diwate, K., Mohite, K., Shinde, M., Rondiya, S., Pawbake, A., Date, A., Pathan, H., Jadkar, S. (2017). Synthesis and Characterization of Chemical Spray Pyrolysed CZTS Thin Films for Solar Cell Applications. *Energy Procedia*, **110**, 180–187. <https://doi.org/10.1016/j.egypro.2017.03.125>
 29. Aditha, S.K., Kurdekar, A.D., Chunduri, L.A.A., Patnaik, S., Kamiseti, V. (2016). Aqueous based reflux method for green synthesis of nanostructures: Application in CZTS synthesis. *MethodsX*, **3**, 35–42. <https://doi.org/10.1016/j.mex.2015.12.003/j.materresbull.2016.10.033>
 30. Pawar, S.M., Pawar, B.S., Moholkar, A.V., Choi, D.S., Yun, J.H., Moon, J.H., Kolekar, S.S., Kim, J.H. (2010). Single step electrosynthesis of $\text{Cu}_2\text{ZnSnS}_4$ (CZTS) thin films for solar cell application. *Electrochimica Acta*, **55(12)**, 4057–4061. <https://doi.org/10.1016/j.electacta.2010.02.051>
 31. Ghosh, A., Thangavel, R. (2014). Experimental and Theoretical Study of Structural and Optical Properties of $\text{Cu}_2\text{ZnSnS}_4$ Nanocrystals for Solar Photovoltaic Applications. *Energy and Environment Focus*, **3(2)**, 157–161. <https://doi.org/10.1166/eef.2014.1074>
 32. Ansari, M.Z., Khare, N. (2014). Structural and optical properties of CZTS thin films deposited by ultrasonically assisted chemical vapour deposition. *Journal of Physics D: Applied Physics*, **47(18)**. <https://doi.org/10.1088/0022-3727/47/18/185101>
 33. Ali, A., Jacob, J., Ashfaq, A., Tamseel, M., Mahmood, K., Amin, N., Hussain, S., Ahmad, W., Rehman, U., Ikram, S., Al-Othmany, D.S. (2019). Modulation of structural, optical and thermoelectric properties of sol-gel grown CZTS thin films by controlling the concentration of zinc. *Ceramics International*, **45(10)**, 12820–12824. <https://doi.org/10.1016/j.ceramint.2019.03.202>
 34. Kannan, A. G., Manjulavalli, T.E., Chandrasekaran, J. (2016). Influence of Solvent on the Properties of CZTS Nanoparticles. *Procedia Engineering*, **141**, 15–22. <https://doi.org/10.1016/j.proeng.2015.08.1112>
 35. Himmrich, M., Haeuselner, H. (1991). Far infrared studies on stannite and wurtzstannite type compounds. *Specmchimica Acta*, **47(7)**.
 36. Fernandes, P.A., Salomé, P.M.P., Da Cunha, A.F. (2011). Study of polycrystalline $\text{Cu}_2\text{ZnSnS}_4$ films by Raman scattering. *Journal of Alloys and Compounds*, **509(28)**, 7600–7606. <https://doi.org/10.1016/j.jallcom.2011.04.097>
 37. Munce, C.G., Parker, G.K., Holt, S.A., Hope, G.A. (2007). A Raman spectroelectrochemical investigation of chemical bath deposited Cu_xS thin films and their modification. *Colloids and Surfaces A: Physicochemical and Engineering Aspects*, **295(1–3)**, 152–158. <https://doi.org/10.1016/j.colsurfa.2006.08.045>
 38. Henry, J., Mohanraj, K., Sivakumar, G. (2016). Electrical and optical properties of CZTS thin films prepared by SILAR method. *Journal of Asian Ceramic Societies*, **4(1)**, 81–84. <https://doi.org/10.1016/j.jascer.2015.12.003>
 39. Mwathe, P., Musembi, R., Munji, M., Odari, V., Munguti, L., Ntilakigwa, A., Nguu, J., Muthoka, B. (2014b). Effect of surface passivation on electrical properties of Pd-F: SnO_2 thin films prepared by spray pyrolysis technique. *Coatings*, **4(4)**, 747–755. <https://doi.org/10.3390/coatings4040747>
 40. Das, S., Sa, K., Alam, I., Mahanandia, P. (2018). Synthesis of CZTS QDs decorated reduced graphene oxide nanocomposite as possible absorber for solar cell. *Materials Letters*, **232**, 232–236. <https://doi.org/10.1016/j.matlet.2018.08.074>
 41. Deepu, D.R., Rajeshmon, V.G., Kartha, C.S., Vijayakumar, K.P. (2014). XPS depth profile study of sprayed CZTS thin films. *AIP Conference Proceedings*, **1591**, 1666–1668. <https://doi.org/10.1063/1.4873070>
 42. Hoflund, G.B., Weaver, J.F., Epling, W.S. (1994). Ag_2O XPS Spectra. *Surface Science Spectra*, **3(2)**, 157–162. <https://doi.org/10.1116/1.1247778>